Critical behavior of the magnetic Weyl semimetal PrAlGe

Wei Liu,[1] Jun Zhao,[2,3] Fanying Meng,[2,3] Azizur Rahman,[3] Yongliang Qin,[2,4] Jiyu Fan,[5] Li Pi,[2,3,4] Zhaoming Tian,[6,*] Haifeng Du,[2,4] Lei Zhang,[2,4,†] and Yuheng Zhang[2,3,4]

[1]*Institutes of Physical Science and Information Technology, Anhui University, Hefei 230601, China*
[2]*Anhui Key Laboratory of Condensed Matter Physics at Extreme Conditions, High Magnetic Field Laboratory, Hefei Institutes of Physical Science, Chinese Academy of Sciences, Hefei 230031, China*
[3]*Hefei National Laboratory for Physical Sciences at the Microscale, University of Science and Technology of China, Hefei 230026, China*
[4]*The High Magnetic Field Laboratory of Anhui Province, Hefei 230031, China*
[5]*Department of Applied Physics, Nanjing University of Aeronautics and Astronautics, Nanjing 210016, China*
[6]*Wuhan National High Magnetic Field Center and School of Physics, Huazhong University of Science and Technology, Wuhan 430074, China*

(Received 7 February 2021; revised 26 March 2021; accepted 17 May 2021; published 1 June 2021)

Noncentrosymmetric PrAlGe is considered to be a magnetic Weyl semimetal that breaks both time-reversal and inversion symmetry, in which the Weyl nodes can be moved by magnetization. However, the magnetic interaction of this system remains poorly understood. In this work we perform a systematical investigation on magnetic properties and critical behaviors in single-crystal PrAlGe. The temperature, field, and angle dependence of magnetization reveal a strong magnetic anisotropy along the c axis and absolute isotropic characteristic in the ab plane. By fitting to the magnetic entropy change $[\Delta S_M(T,H)]$ around the critical temperature $T_C = 16$ K, critical exponents $\beta = 0.136(6)$, $\gamma = 1.801(7)$, and $\delta = 14.2(6)$ are obtained. Based on the obtained critical exponents, $\Delta S_M(T,H)$ and $M(T,H)$ curves are scaled into universality curves under the framework of universality principle. The critical behaviors and exponents suggest that the magnetic interaction in PrAlGe is of a two-dimensional Ising type, revealing a uniaxial magnetic interaction along the c axis. However, the ordering moments are tilted from the c axis, which causes antiferromagnetism in the ab plane. The clarification of the magnetic interaction and magnetic structure is of significance for unveiling its interplay with topological properties in this system.

DOI: 10.1103/PhysRevB.103.214401

I. INTRODUCTION

Topological semimetals have been one of the major discoveries in condensed-matter physics in recent years, exhibiting fascinating properties such as high carrier mobility [1,2], extremely large positive transverse magnetoresistance [2–4], negative magnetoresistance [5], transport response and chiral anomaly [6], anomalous Hall effect (AHE) [7,8], etc. In particular, the magnetic Weyl semimetal, in which the Weyl nodes can be generated and modulated by magnetization, provides an ideal platform for the investigation of the magnetic field-tunable link between Weyl physics and magnetism [9]. Furthermore, in such systems, large magnetically sensitive anomalous transport responses are expected as the magnetism can break time-reversal symmetry and therefore can be applied in topological spintronics [10]. Compared with the rapid development of nonmagnetic semimetals in theoretical prediction and experimental confirmation [3,11–16], only a few systems such as GdPtBi [17–19] and $Co_3Sn_2S_2$ [8,20] have been experimentally verified for magnetic Weyl semimetals. Due to lack of appropriate or high quality specimens, most of the theoretically expected magnetic Weyl semimetals have not been experimentally confirmed [21–24]. Therefore, exploration of new magnetic semimetals is therefore of great importance.

Recently, noncentrosymmetric structure RAlGe (R = Ce, Pr) with space group $I4_1md$ have been predicted to be magnetic Weyl semimetals [25]. While their isostructural compounds LaAlGe have been confirmed to be a nonmagnetic type-II Weyl semimetal by photoemission [26]. In the meantime, CeAlGe is proposed as magnetic type-II Weyl semimetal without AHE due to an antiferromagnetic (AFM) ground state [27]. Since both space-inversion symmetry and time-reversal symmetry broken, PrAlGe is supposed to be a type-I Weyl semimetal with an easy axis along the c axis [25]. Magnetic and transport measurements show that PrAlGe has a ferromagnetic (FM) order along the c axis and a large AHE up to $\sim 680\ \Omega^{-1}\,\mathrm{cm}^{-1}$ originating from the contribution of the intrinsic Karplus-Luttinger mechanism [28]. Moreover, recent spectroscopy and transport measurements have directly revealed a linear energy dispersion of the Weyl fermions and the large anomalous Hall response, which support the topological characteristics of Weyl fermions in this system [29].

Up to date, research on PrAlGe mainly focuses on transport [28–31] and structure properties [31]. To realize the modulation of the topological properties by magnetization, the

*Corresponding author: tianzhaoming@hust.edu.cn
†Corresponding author: zhanglei@hmfl.ac.cn

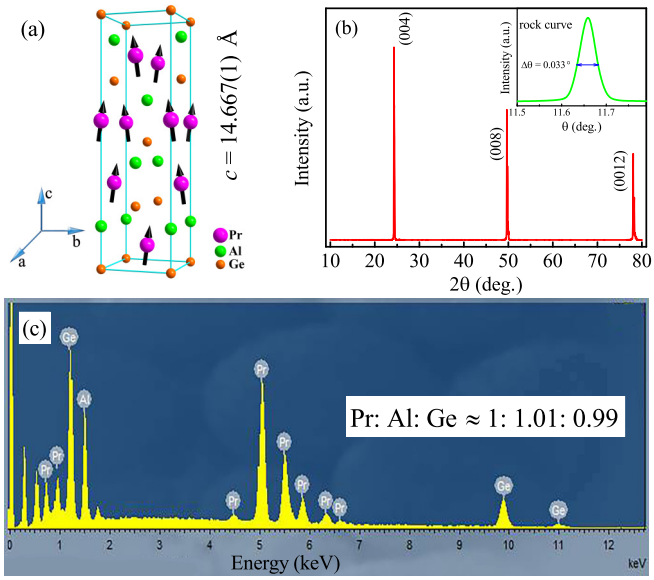

FIG. 1. (a) Crystal structure of PrAlGe. (b) XRD pattern of the single-crystal PrAlGe (inset gives the rocking curve). (c) EDX spectrum for single-crystal PrAlGe.

clarification of magnetic interactions and magnetic structure is highly desirable. Motivated by this, we systematically investigate the magnetism of single-crystal PrAlGe. Based on the anisotropic magnetization, magnetic entropy change, and critical behaviors, strong anisotropic magnetic interaction is unveiled and the magnetic structure is constructed for the PrAlGe system.

II. EXPERIMENTAL METHODS

Single crystals of PrAlGe were prepared by a self-flux technique using extra Al as a flux [32]. The detailed growth process was described in a previous report [28]. The crystal structure of PrAlGe was checked by the x-ray diffraction (XRD), performed on a Rigaku-TTR3 x-ray diffractometer, with high intensity graphite monochromatized Cu $K\alpha$ radiation. The chemical compositions of the single crystal were checked by energy dispersive x-ray (EDX) spectrometry. The magnetization measurements, including the angle-, temperature-, and field-dependent magnetization, were carried out by a Quantum Design vibrating sample magnetometer (SQUID-VSM). In order to obtain the magnetic entropy change, the initial isothermal magnetization with field applied along the c axis ($H//c$) was measured. Before each measurement of initial isothermal magnetization, the sample was heated to room temperature and held for 2 min, then cooled to the target temperature under zero field. The magnetic field was relaxed before data collection, and a no-overshoot mode was applied to ensure a precise magnetic field. The magnetization under high magnetic field beyond 7 T was performed on the water-cooling resistive magnet.

III. RESULTS AND DISCUSSION

PrAlGe belongs to the space group $I4_1md$ with noncentrosymmetric features as illustrated in Fig. 1(a). Figure 1(b) shows the XRD pattern of the as-synthesized sample, where the series of sharp diffraction peaks corresponds well to the (0 0 l) plane of PrAlGe single crystals. The determined lattice parameter is $c = 14.667(1)$ Å, which is consistent with the values reported previously [28,30,31]. The high resolution x-ray rocking curve shown in the inset of Fig. 1(b) gives that the full-width at half-maximum (FWHM) is $\Delta\theta = 0.033°$. The single peak and narrow FWHM of the rocking curve indicate the superior crystalline quality of the single crystal used. Figure 1(c) depicts the EDX spectrum for the single-crystal PrAlGe, where the chemical proportions are determined as Pr : Al : Ge = 1 : 1.01 : 0.99 approaching closely the desired proportion.

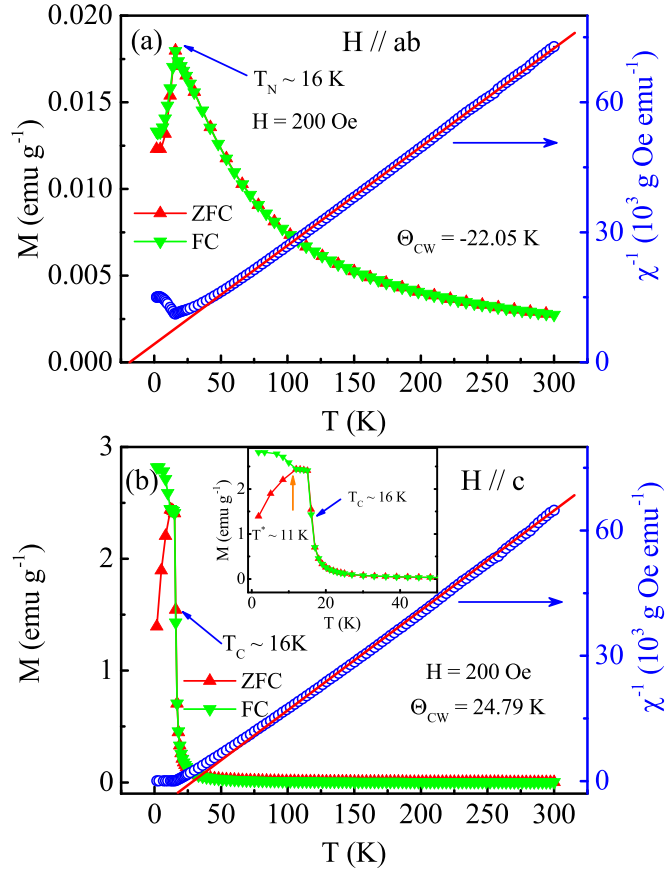

FIG. 2. Temperature-dependent magnetization with (a) $H//ab$ and (b) $H//c$ (inset magnifies the phase transition region for $H//c$).

Figures 2(a) and 2(b) display the temperature dependence of magnetization [$M(T)$] (left axis) and the reciprocal of susceptibility [$\chi^{-1}(T)$] (right axis) for single-crystal PrAlGe with field parallel to the ab plane ($H//ab$) and c axis ($H//c$), respectively. The $M(T)$ curves were measured under zero field cooling (ZFC) and field cooling (FC) sequences. Apparently, $M(T)$ curves for $H//ab$ and $H//c$ exhibit very distinctive behaviors. When $H//ab$, peaks appear on both ZFC and FC $M(T)$ curves, which coincide with each other even at low temperature. These features suggest a typical paramagnetic-to-antiferromagnetic (PM-AFM) phase transition, where the Néel temperature is determined as $T_N \sim 16$ K. However, when $H//c$, $M(T)$ curves display a λ shape due to the bifurcation between ZFC and FC curves. The $M(T)$ curves with $H//c$

implies a feature of paramagnetic-to-ferromagnetic (PM-FM) phase transition, where the Curie temperature is determined as $T_C \sim 16$ K. In addition, magnetization values with $H//c$ are much larger than those with $H//ab$ by two orders of magnitude, indicating strong magnetic anisotropy in PrAlGe. The $\chi^{-1}(T)$ plotted as the right axis in Figs. 2(a) and 2(b) present straight lines above the phase transition temperature, suggesting paramagnetic behaviors for both $H//ab$ and $H//c$ in the high temperature region. The fittings of $\chi^{-1}(T)$ curves by the Curie-Weiss law $[\chi(T) = C/(T - \Theta_{CW})]$ give the Curie-Weiss temperature $\Theta^{ab}_{CW} = -22.05$ K for $H//ab$ and $\Theta^{c}_{CW} = 24.79$ K for $H//c$, respectively. The negative Θ_{CW} confirms an AFM coupling for $H//ab$, while the positive one suggests an FM coupling for $H//c$. As shown in the inset of Fig. 2(b), another anomaly is noted in the $M(T)$ curves for $H//c$ at around 11 K, which indicates another magnetic transition [31]. The magnetic behaviors here are well consistent with previous reports [28–31].

Figure 3(a) shows the field dependence of magnetization $[M(H)]$ up to 30 T at $T = 1.8$, 14, 16, and 18 K for $H//ab$ and $H//c$, where $M(H)$ curves for $H//ab$ and $H//c$ exhibit absolutely different behaviors. As the field increases, the $M(H)$ curve with $H//ab$ increases linearly and shows a nonsaturated behavior even up to 30 T. However, the $M(H)$ curve with $H//c$ increases rapidly with the increase of field in the low field region, and reaches saturation rapidly when H exceeds 4.3 kOe for that at 1.8 K. The $M(H)$ curves in Fig. 3(a) suggest strong magnetic anisotropic properties of PrAlGe. In order to unveil the evolution of the magnetic anisotropy, the angle dependence of magnetization $[M(\varphi)]$ was performed at 2 K, which is presented as a three-dimensional (3D) plot in Fig. 3(b). The in-plane $M(\varphi)$ curves are measured by the applied field rotated within the ab plane, which is depicted in the xy plane. The out-of-plane $M(\varphi)$ curves are performed with the field rotated from the c axis to the ab plane, which are projective to the xz plane. As can be seen in Fig. 3(b), all in-plane $M(\varphi)$ curves exhibit circular patterns despite orientations of the magnetic field, which suggest absolutely isotropic magnetism in the ab plane. The out-of-plane magnetic behaviors are totally different. All curves reach the maximum when $H//c$ while the minimum when $H//ab$, illustrating dumbbell shapes. The strong magnetization along the c axis reveals that the easy axis of magnetization is along the c axis. The $M(T)$, $M(H)$, and $M(\varphi)$ curves uncover strong magnetic anisotropy along the c axis in single-crystal PrAlGe, which is beneficial to its potential application in spintronics [33].

In view of the strong magnetic anisotropy along the c axis in single-crystal PrAlGe, it is significant to explore the magnetic couplings and interactions. In the case of a magnetic phase transition, the magnetic entropy change is correlated intrinsically with critical exponents, which is an effective method to unveil the magnetic interactions [34]. The critical exponents can be obtained by means of magnetic entropy change, which generates the exponents but does not require any initial parameters compared with other methods [35,36]. The initial isothermal magnetization $[IM(H)]$ around T_C with $H//c$ are measured in detail to generate the magnetic entropy change, as given in Fig. 4(a). Before measuring $IM(H)$ curves, the sample was heated to room temperature and held for 2 min. Each $IM(H)$ curve was performed when the sample

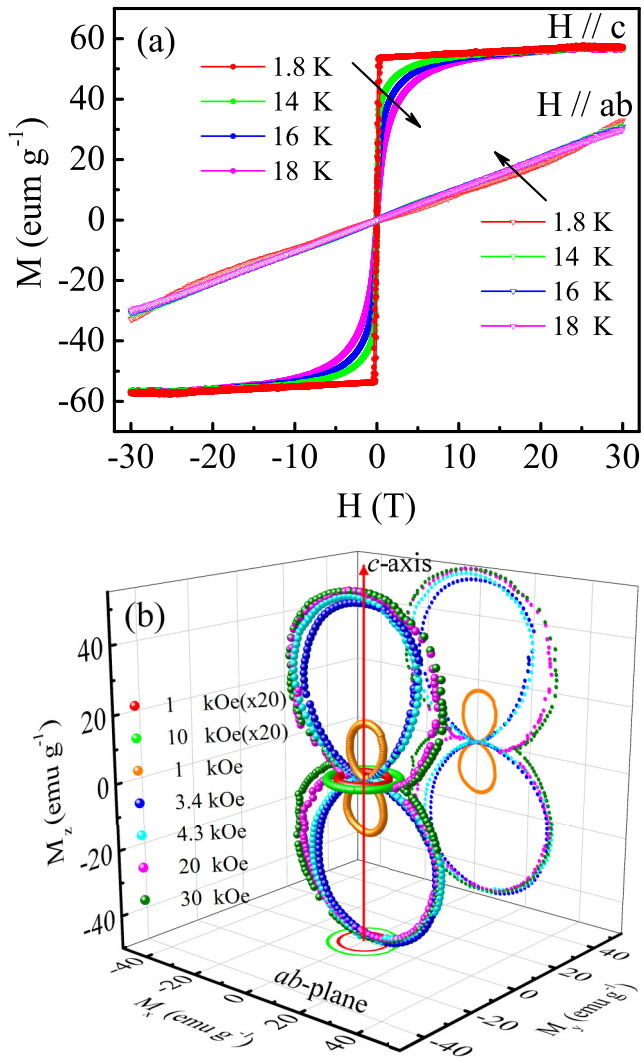

FIG. 3. (a) Field dependence of isothermal magnetization $[M(H)]$ up to 30 T at $T = 1.8$, 14, 16, and 18 K with $H//ab$ and $H//c$. (b) 3D plot of angle-dependent magnetization $[M(\varphi)]$ at $T = 2$ K under selected field: in-plane $M(\varphi)$ (xy plane) with H rotated within the ab plane; out-of-plane $M(\varphi)$ (xz plane) with H rotated from the ab plane to the c axis.

was cooled to the target temperature under zero field. The $IM(H)$ curves were carried out with temperature intervals of $\Delta T = 1$ K around T_C. As shown in Fig. 4(a), all $IM(H)$ curves show similar saturation behaviors below T_C, while they increase as the field increases above T_C indicating nonsaturated behaviors. The magnetic entropy change $[\Delta S_M(T, H)]$ induced by the external field can be expressed as [37,38]

$$\Delta S_M(T, H) = S_M(T, H) - S_M(T, 0) = \int_0^{H^{\max}} \left[\frac{\partial M(T, H)}{\partial T}\right]_H dH, \quad (1)$$

where $H^{\max}$ is the maximum of external magnetic field. According to Eq. (1), the temperature-dependent magnetic entropy change $[\Delta S_M(T)]$ under different fields can be obtained, as plotted in Fig. 4(b). Each $-\Delta S_M(T)$ curve shows a peak at $T_C \sim 16$ K, indicating that the magnetic entropy change

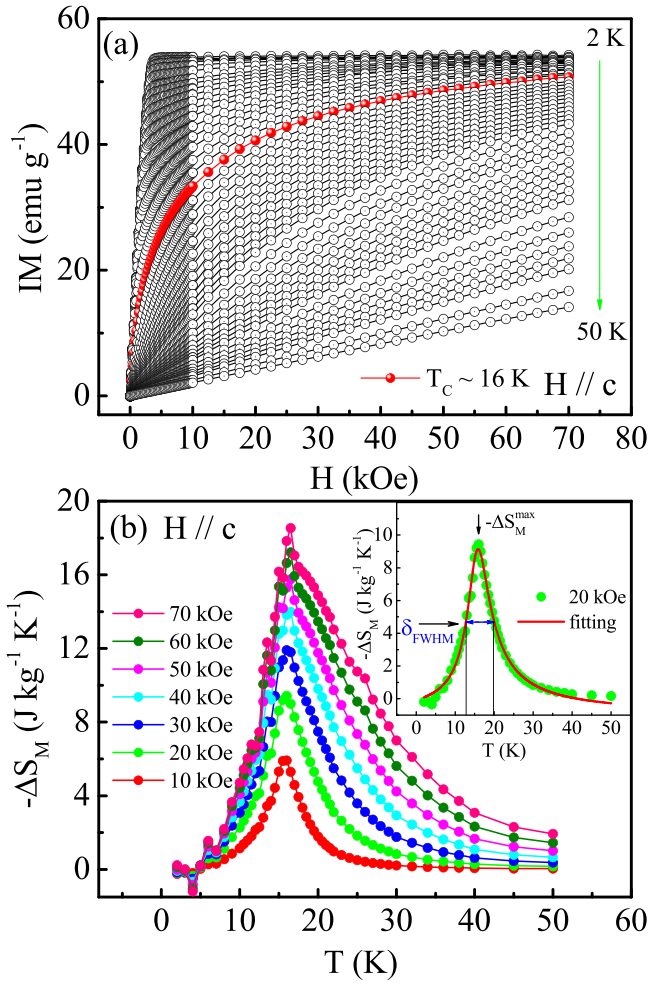

FIG. 4. (a) Field dependence of isothermal initial magnetization [$IM(H)$] around T_C with $H//c$. (b) Temperature dependence of magnetic entropy change [$-\Delta S_M(T)$] under different field with $H//c$ (inset shows definitions of the generated parameters of a typical fitting).

reaches the maximum at the phase transition temperature. The $-\Delta S_M(T)$ curves can be fitted by the functions as shown in the inset of Fig. 4(b), which generate parameters of the maximum of $|\Delta S_M(T)|$ ($|\Delta S_M^{\max}|$) and the full-width at half-maximum (δ_{FWHM}). The inset of Fig. 4(b) gives the definitions of the parameters.

As the field increases, parameters of $|\Delta S_M(T,H)|$ curve follow a series of power laws [34,39]:

$$|\Delta S_M^{\max}| \propto H^n, \quad \delta_{\mathrm{FWHM}} \propto H^b, \quad RCP(S) \propto H^c, \tag{2}$$

where $RCP(S)$ is relative cooling power defined as $RCP(S) = |\Delta S_M^{\max}\delta_{\mathrm{FWHM}}|$. Figures 5(a)–5(c) plot the field dependence of $|\Delta S_M^{\max}|$, δ_{FWHM}, and $RCP(S)$ for $H//c$, the fittings of which give that $n = 0.554(6)$, $b = 0.515(4)$, and $c = 1.070(5)$. Furthermore, exponents n, b, and c are associated with critical exponents β, γ, δ, and Δ [40]:

$$n = 1 + \frac{\beta - 1}{\beta + \gamma}, \quad b = \frac{1}{\Delta}, \quad c = 1 + \frac{1}{\delta}, \tag{3}$$

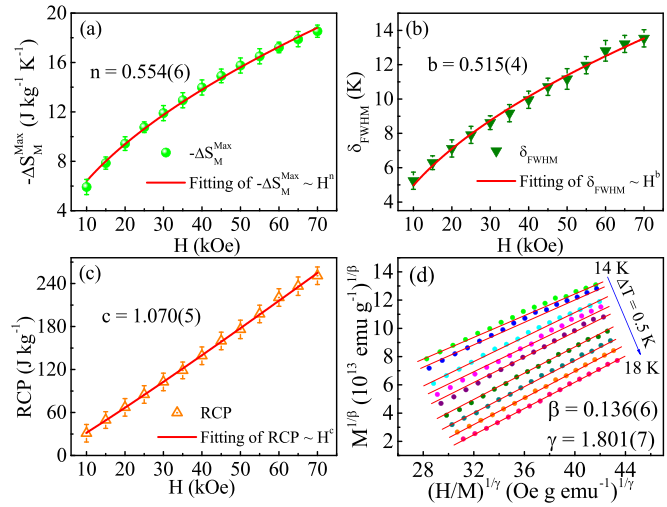

FIG. 5. Field-dependent parameters of $\Delta S_M(T)$ for $H//c$: (a) $-\Delta S_M^{\max}$, (b) δ_{FWHM}, (c) RCP, and (d) modified Arrott plot (MAP).

where β is associated with the spontaneous magnetization, γ is corresponding to the initial susceptibility, and δ is correlating with the critical magnetization. In addition, these critical exponents should fulfill the Widom scaling law [41]:

$$\delta = 1 + \frac{\gamma}{\beta}. \tag{4}$$

Combining Eqs. (3) and (4), critical exponents for single-crystal PrAlGe are obtained as $\beta = 0.136(6)$, $\gamma = 1.801(7)$ and $\delta = 14.2(6)$ for $H//c$.

The reliability of the obtained critical exponents can be verified by the modified Arrott plot (MAP). According to the Arrott-Noakes equation of state, there is [42]

$$(H/M)^{1/\gamma} = (T - T_C)/T_C + (M/M_1)^{1/\beta}, \tag{5}$$

where M_1 is a constant. The Arrott-Noakes equation of state suggests that $M^{1/\beta}$ vs $(H/M)^{1/\gamma}$ should be a bunch of straight lines parallel to each other, which constitute the MAP. Figure 5(d) plots the MAP for single-crystal PrAlGe with $H//c$. All the curves of MAP exhibit a series of lines parallel to each other under high field, which confirms reliability of the obtained critical exponents. On the other hand, the critical exponent δ can also be independently fitted out by the critical isothermal analysis at $T = T_C$:

$$M = DH^{1/\delta}, \tag{6}$$

where D is critical amplitude. The slope of $\log(M)$ vs $\log(H)$ at T_C gives $1/\delta$. Figure 6 plots the isothermal magnetization at T_C up to high magnetic field of 30 T. The inset of Fig. 6 on log-log scale gives the fitting exponent $\delta = 14.41(6)$. The independently obtained δ by the critical isothermal analysis is in agreement with that obtained by the magnetic entropy change, confirming the reliability of the obtained critical exponents.

According to the universality principle, $\Delta S_M(T,H)$ can be scaled into a universal curve regardless of the external field [34]. The magnetic entropy change can be normalized as $\Delta S'_M = \Delta S_M/\Delta S_M^{\max}$. The temperature is normalized to be

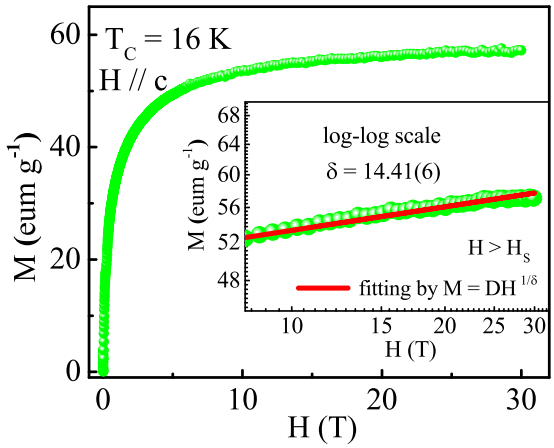

FIG. 6. Isothermal magnetization at T_C up to high magnetic field of 30 T (inset shows that on log-log scale with the fitting line).

a rescaled temperature θ defined as [40]

$$\theta = \begin{cases} \theta_- = (T_C - T)/(T_{r1} - T_C), & T \leqslant T_C, \\ \theta_+ = (T - T_C)/(T_{r2} - T_C), & T > T_C, \end{cases} \tag{7}$$

where T_{r1} and T_{r2} are reference temperatures below and above T_C, respectively, which correspond to $\Delta S_M(T_{r1}, T_{r2}) = \frac{1}{2}\Delta S_M^{\max}$. Figure 7(a) shows $\Delta S'_M(\theta)$ curves. All curves collapse into a single universal curve independent of the external field, where T_{r1} and T_{r2} are corresponding to $\theta = -1$ and $\theta = +1$. Meanwhile, the $\Delta S_M(T, H)$ can be also scaled by another scaled equation of state $H/M^\delta = f(\varepsilon/M^{1/\beta})$, based on which $\Delta S_M(T, H)$ can be rewritten as [43,44]

$$\Delta S_M(T, H) = H^{\frac{1-\alpha}{\Delta}} g\Big(\frac{\varepsilon}{H^{1/\Delta}}\Big), \tag{8}$$

where critical exponents α and Δ can be yielded by the Rushbrooke's law [45]:

$$\alpha = 2 - 2\beta - \gamma, \quad \Delta = \delta\beta. \tag{9}$$

Subsequently, $\alpha = -0.074(9)$ and $\Delta = 1.937(5)$ are obtained according to Eqs. (9). Figure 7(b) gives $-\Delta S_M/H^{(1-\alpha)/\Delta}$ vs $\varepsilon/H^{1/\Delta}$, where all the curves collapse onto a single universal curve with the exception of a bit of divergence below T_C. For this divergence confirmed in the inset of Fig. 2(b), it may be due to an abnormal spin transition which occurs at 11 K for the single-crystal PrAlGe. Puphal and Destraz *et al.* attribute this to a spin reorientation [10,31,46]. However, the measurement of ac susceptibility by Meng *et al.* rules out the spin-glassy transition [28].

In addition, the reliability of the critical exponents can also be examined by the scaling functions, one of which is described as [47]

$$M(H, \varepsilon) = \varepsilon^\beta f_\pm(H/\varepsilon^{\beta+\gamma}), \tag{10}$$

where the reduced temperature is defined as $\varepsilon = (T - T_C)/T_C$, and f_+ for $T > T_C$ and f_- for $T < T_C$ are regular functions. In terms of the renormalized magnetization $m \equiv \varepsilon^{-\beta} M(H, \varepsilon)$ and renormalized field $h \equiv H\varepsilon^{-(\beta+\gamma)}$, the scaling function can be rewritten as $m = f_\pm(h)$, which indicates that m vs h curves will form two separate branches above and below T_C, respectively. Figure 8(a) depicts $m(h)$ curves, all of which

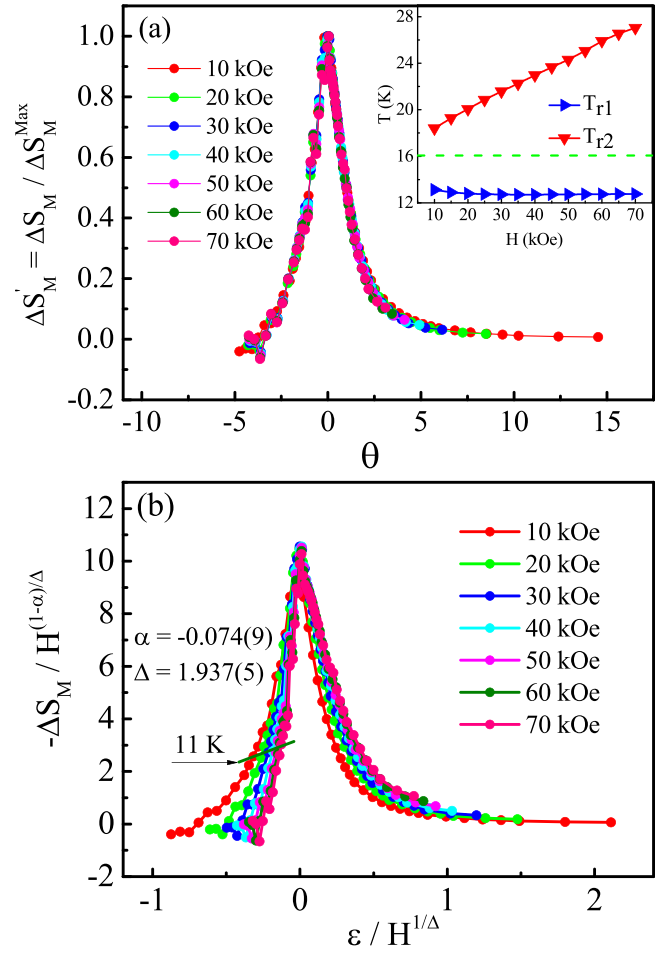

FIG. 7. (a) Normalization of $\Delta S_M(T)$ vs rescaling temperature θ (inset shows field dependence of the reference temperature T_r). (b) Scaling of $\Delta S_M(T)$ under the obtained critical exponents.

collapse onto two branches above and below T_C. Meanwhile, the scaling functions can be written into another form [47]:

$$\frac{H}{M^\delta} = h\Big(\frac{\varepsilon}{M^{1/\beta}}\Big), \tag{11}$$

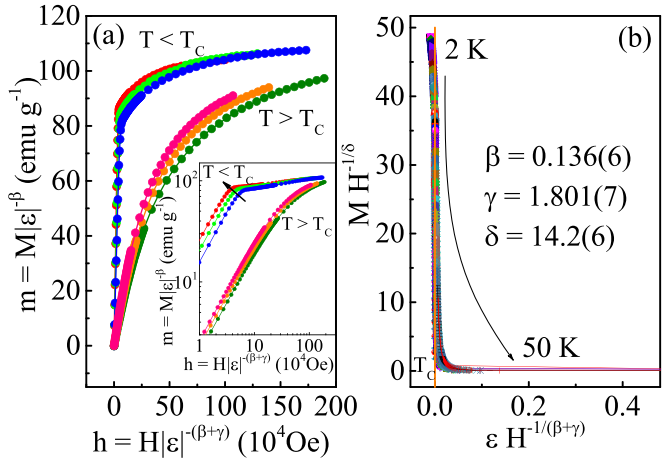

FIG. 8. (a) Scaling of $M(H)$ curves around the phase transition temperature into $m(h)$. (b) $MH^{-1/\delta}$ vs $\varepsilon H^{-1/(\beta+\gamma)}$.

TABLE I. Critical exponents of PrAlGe and different theoretical models.

Composition	Technique	Ref.	T_C	β	γ	δ
PrAlGe	Experiment	This work	16	0.136(6)	1.801(7)	14.2(6)
2D Ising	Theory	[48]	–	0.125	1.75	15
3D Ising	Theory	[47]	–	0.325	1.24	4.82
3D XY	Theory	[47]	–	0.346	1.316	4.81
Mean field	Theory	[47]	–	0.5	1.0	3.0
3D Heisenberg	Theory	[47]	–	0.365	1.386	4.8
Tricritical mean field	Theory	[49]	–	0.25	1.0	5.0

where $h(x)$ is a scaling function. This scaling hypothesis implies that all the $M(H)$ curves including $T < T_C$ and $T > T_C$ would collapse onto a single curve of $MH^{-1/\delta}$ vs $\varepsilon H^{-1/(\beta+\gamma)}$. As shown in Fig. 8(b), all the curves are scaled into a single curve with T_C located at the origin. The above results ambiguously confirm that the critical exponents obtained here are self-consistent, reliable, and intrinsic.

The obtained critical exponents of PrAlGe, as well as those of theoretical models, are listed in Table I for a better comparison. The critical exponents of PrAlGe are mostly close to those of a two-dimensional (2D) Ising model, especially δ. The critical exponent δ of a 2D-Ising model ($\delta = 15$) differs greatly with other models (see Table I). The independently obtained $\delta = 14.2(6)$ by the magnetic entropy change and $\delta = 14.41(6)$ by the critical isothermal analysis are both close to that of the 2D-Ising model. Taking into consideration the three critical exponents, it indicates a 2D-Ising-like magnetic coupling in single-crystal PrAlGe. The interaction of 2D-Ising type gives $d = 2$ and $n = 1$ (d is the spatial dimensionality and n is the spin dimensionality), which implies a two-dimensional characteristic in structure and a one-dimensional interaction in magnetism. Other reports also show the Ising-like magnetic coupling for PrAlGe [10,28]. Indeed, the structure of PrAlGe is anisotropic, where the lattice constants $a = b = 4.2368$ Å and $c = 14.609$ Å [28]. The 2D-Ising interaction in a 3D material is also reported in other systems. For example, in three-dimensional uranium ferromagnet URhAl, 2D-Ising type of magnetic coupling interactions is revealed, where such low-dimensional magnetic coupling results from the strong hybridization between the uranium $5f$ and rhodium $4d$ electrons in the U-Rh_I layer [50]. Similarly, in its isostructural URhGa and UCoGa, critical exponents determined by analyzing magnetization data point to the 2D-Ising universality class [51]. Moreover, 2D-Ising-like critical behavior is also found in a three-dimensional uniaxial ferroelectric $Sr_{0.61}Ba_{0.39}Nb_2O_6$ [52]. Meanwhile, for PrAlGe, an AFM characteristic is also noted in the *ab* plane. The magnetization and magnetic anisotropy are previously investigated in other literature [10,28–31]. Based on the previous reports and the present results of critical behavior, the magnetic structure of PrAlGe is sketched in Fig. 1(a). All moments are ferromagnetically arranged along the *c* axis, illustrating an FM behavior. However, the moments are tilted from the *c* axis to the *ab* plane, which result in AFM arrangement in the *ab* plane. Consequently, PrAlGe exhibits an FM along the *c* axis while an AFM ordering in the *ab* plane, which exactly explains its anisotropic magnetism. In fact, Destraz *et al.* evidence that in part of the sample Pr moments tilt away from the *c* axis over nanometric length scale, which they attribute to large FM domain walls [10]. In addition, the Ising-like interaction is also revealed by neutron scattering experiments and magnetic anisotropy measurements [10,28]. It should be noted that the magnetic interaction is complex which can be affected and modulated by the internal and external facts such as defects, field, pressure, temperature, and so on. Therefore, the results obtained here are confined within the temperature range around T_C under external field.

For the investigation and modulation of topological properties in PrAlGe, the clarification of magnetic interactions and magnetic structure is of great importance. As we know, the magnetic interaction and spin-orbital coupling play an important role in the formation and evolution of topological nontrivial states. In PrAlGe, the intrinsic FM ordering acts as a Zeeman coupling to split the spin-up and spin-down bands. However, the whole band structure is still kept. The split of bands makes the Weyl nodes in k space shift to break time-reversal symmetry, which consequently generates a large anomalous Hall effect [25]. Many other novel phenomena are also expected in magnetic Weyl semimetal due to the direct interplay between Weyl nodes and incommensurate magnetism [53]. More and more studies have suggested that the magnetic structure and magnetic interaction are essential in these processes. Recently, it is proposed that a Dirac semimetal state exists in the AFM ground state and a Weyl semimetal state appears in the FM state in rare-earth monopnictides NdSb [54,55]. Furthermore, it has been confirmed that many magnetic incommensurate phases exist in the magnetic Weyl semimetal candidate CeAlGe, which confirm connections between magnetism and topologically nontrivial states [53]. As for PrAlGe, small-angle neutron scattering (SANS) measurements indicate that it could be a platform for the study of Weyl fermion gauge fields arising from spatially inhomogeneous magnetism [10]. The investigations in the present work therefore provide a comprehensive understanding of the magnetism in Weyl semimetal PrAlGe, which is significant for understanding the interplay between the magnetism and topological properties in this system.

IV. CONCLUSION

In summary, the magnetism and critical behavior of single-crystal PrAlGe are systematically investigated. The magnetic properties, including $M(T)$, $M(\varphi)$, and $M(H)$ with the field along different crystallographic directions, reveal strong

magnetic anisotropy along the *c* axis and absolutely isotropy in the *ab* plane. The critical behavior suggests that the magnetic coupling in single-crystal PrAlGe is of an Ising-like type. Our present work provides a comprehensive understanding of the magnetic structure and interaction in Weyl semimetal PrAlGe.

ACKNOWLEDGMENTS

The authors thank Dr. W. Tong, L. S. Ling, and C. Y. Xi for the measurement of magnetization under High Magnetic Field Facility. This work was supported by the National Key R&D Program of China (Grant No. 2017YFA0303201), the National Natural Science Foundation of China (Grants No. 12074386, No. 11874358, No. 11874158, No. U1732276, No. 11974181, and No. 11574322), the Users with Excellence Program of Hefei Science Center CAS (2019HSC-UE010), Anhui University Scientific Research Startup Fund (No. S020318006/023), the Key Project of Natural Scientific Research of Universities in Anhui Province (No. K120462009), and the open research program from Science and Technology Commission of Shanghai Municipality (Grant No. 19DZ2270200). A proportion of this work was supported by the High Magnetic Field Laboratory of Anhui Province.

[1] T. Liang, Q. Gibson, M. N. Ali, M. Liu, R. J. Cava, and N. P. Ong, Nat. Mater. **14**, 280 (2015).
[2] C. Shekhar, A. K. Nayak, Y. Sun, M. Schmidt, M. Nicklas, I. Leermakers, U. Zeitler, Y. Skourski, J. Wosnitza, Z. Liu, Y. Chen, W. Schnelle, H. Borrmann, Y. Grin, C. Felser, and B. Yan, Nat. Phys. **11**, 645 (2015).
[3] M. N. Ali, J. Xiong, S. Flynn, J. Tao, Q. D. Gibson, L. M. Schoop, T. Liang, N. Haldolaarachchige, M. Hirschberger, N. P. Ong, and R. J. Cava, Nature (London) **514**, 205 (2014).
[4] N. Kumar, Y. Sun, N. Xu, K. Manna, M. Yao, V. Süss, I. Leermakers, O. Young, T. Förster, M. Schmidt, H. Borrmann, B. Yan, U. Zeitler, M. Shi, C. Felser, and C. Shekhar, Nat. Commun. **8**, 1642 (2017).
[5] X. Huang, L. Zhao, Y. Long, P. Wang, D. Chen, Z. Yang, H. Liang, M. Xue, H. Weng, Z. Fang, X. Dai, and G. Chen, Phys. Rev. X **5**, 031023 (2015).
[6] S. Jia, S.-Y. Xu, and M. Z. Hasan, Nat. Mater. **15**, 1140 (2016).
[7] T. Suzuki, R. Chisnell, A. Devarakonda, Y.-T. Liu, W. Feng, D. Xiao, J. W. Lynn, and J. Checkelsky, Nat. Phys. **12**, 1119 (2016).
[8] E. Liu, Y. Sun, N. Kumar, L. Muechler, A. Sun, L. Jiao, S.-Y. Yang, D. Liu, A. Liang, Q. Xu, J. Kroder, V. Süß, H. Borrmann, C. Shekhar, Z. Wang, C. Xi, W. Wang, W. Schnelle, S. Wirth, Y. Chen *et al.*, Nat. Phys. **14**, 1125 (2018).
[9] Y. Tokura, M. Kawasaki, and N. Nagaosa, Nat. Phys. **13**, 1056 (2017).
[10] D. Destraz, L. Das, S. S. Tsirkin, Y. Xu, T. Neupert, J. Chang, A. Schilling, A. G. Grushin, J. Kohlbrecher, L. Keller, P. Puphal, E. Pomjakushina, and J. S. White, npj Quantum Mater. **5**, 5 (2020).
[11] B. Q. Lv, H. M. Weng, B. B. Fu, X. P. Wang, H. Miao, J. Ma, P. Richard, X. C. Huang, L. X. Zhao, G. F. Chen, Z. Fang, X. Dai, T. Qian, and H. Ding, Phys. Rev. X **5**, 031013 (2015).
[12] Z. K. Liu, B. Zhou, Y. Zhang, Z. J. Wang, H. M. Weng, D. Prabhakaran, S.-K. Mo, Z. X. Shen, Z. Fang, X. Dai, Z. Hussain, and Y. L. Chen, Science **343**, 864 (2014).
[13] S.-Y. Xu, I. Belopolski, N. Alidoust, M. Neupane, G. Bian, C. Zhang, R. Sankar, G. Chang, Z. Yuan, C.-C. Lee, S.-M. Huang, H. Zheng, J. Ma, D. S. Sanchez, B. Wang, A. Bansi, F. Chou, P. P. Shibayev, H. Lin, S. Jia *et al.*, Science **349**, 613 (2015).
[14] Q. Li, D. E. Kharzeev, C. Zhang, Y. Huang, I. Pletikosić, A. V. Fedorov, R. D. Zhong, J. A. Schneeloch, G. D. Gu, and T. Valla, Nat. Phys. **12**, 550 (2016).
[15] Y. Wu, D. Mou, N. H. Jo, K. Sun, L. Huang, S. L. Bud'ko, P. C. Canfield, and A. Kaminski, Phys. Rev. B **94**, 121113(R) (2016).
[16] X. Zhou, Q. Liu, Q. S. Wu, T. Nummy, H. Li, J. Griffith, S. Parham, J. Waugh, E. Emmanouilidou, B. Shen, O. V. Yazyev, N. Ni, and D. Dessau, Phys. Rev. B **97**, 241102(R) (2018).
[17] M. Hirschberger, S. Kushwaha, Z. Wang, Q. Gibson, S. Liang, C. A. Belvin, B. A. Bernevig, R. J. Cava, and N. P. Ong, Nat. Mater. **15**, 1161 (2016).
[18] N. Kumar, S. N. Guin, C. Felser, and C. Shekhar, Phys. Rev. B **98**, 041103(R) (2018).
[19] F. Hütt, A. Yaresko, M. B. Schilling, C. Shekhar, C. Felser, M. Dressel, and A. V. Pronin, Phys. Rev. Lett. **121**, 176601 (2018).
[20] D. F. Liu, A. J. Liang, E. K. Liu, Q. N. Xu, Y. W. Li, C. Chen, D. Pei, W. J. Shi, S. K. Mo, P. Dudin, T. Kim, C. Cacho, G. Li, Y. Sun, L. X. Yang, Z. K. Liu, S. S. P. Parkin, C. Felser, and Y. L. Chen, Science **365**, 1282 (2019).
[21] X. Wan, A. M. Turner, A. Vishwanath, and S. Y. Savrasov, Phys. Rev. B **83**, 205101 (2011).
[22] G. Xu, H. Weng, Z. Wang, X. Dai, and Z. Fang, Phys. Rev. Lett. **107**, 186806 (2011).
[23] P. Tang, Q. Zhou, G. Xu, and S.-C. Zhang, Nat. Phys. **12**, 1100 (2016).
[24] G. Hua, S. Nie, Z. Song, R. Yu, G. Xu, and K. Yao, Phys. Rev. B **98**, 201116(R) (2018).
[25] G. Chang, B. Singh, S.-Y. Xu, G. Bian, S.-M. Huang, C.-H. Hsu, I. Belopolski, N. Alidoust, D. S. Sanchez, H. Zheng, H. Lu, X. Zhang, Y. Bian, T.-R. Chang, H.-T. Jeng, A. Bansil, H. Hsu, S. Jia, T. Neupert, H. Lin *et al.*, Phys. Rev. B **97**, 041104(R) (2018).
[26] S.-Y. Xu, N. Alidoust, G. Chang, H. Lu, B. Singh, I. Belopolski, D. S. Sanchez, X. Zhang, G. Bian, H. Zheng, M.-A. Husanu, Y. Bian, S.-M. Huang, C.-H. Hsu, T.-R. Chang, H.-T. Jeng, A. Bansil, T. Neupert, V. N. Strocov, H. Lin *et al.*, Sci. Adv. **3**, e1603266 (2017).
[27] H. Hodovanets, C. J. Eckberg, P. Y. Zavalij, H. Kim, W.-C. Lin, M. Zic, D. J. Campbell, J. S. Higgins, and J. Paglione, Phys. Rev. B **98**, 245132 (2018).
[28] B. Meng, H. Wu, Y. Qiu, C. Wang, Y. Liu, Z. Xia, S. Yuan, H. Chang, and Z. Tian, APL Mater. **7**, 051110 (2019).
[29] D. S. Sanchez, G. Chang, I. Belopolski, H. Lu, J.-X. Yin, N. Alidoust, X. Xu, T. A. Cochran, X. Zhang, Y. Bian, S. S., Zhang, Y.-Y. Liu, J. Ma, G. Bian, H. Lin, S.-Y. Xu, S. Jia, and M. Z. Hasan, Nat. Commun. **11**, 3356 (2020).
[30] H.-Y. Yang, B. Singh, B. Lu, C.-Y. Huang, F. Bahrami, W.-C. Chiu, D. Graf, S.-M. Huang, B. Wang, H. Lin, D. Torchinsky, A. Bansil, and F. Tafti, APL Mater. **8**, 011111 (2020).

[31] P. Puphal, C. Mielke, N. Kumar, Y. Soh, T. Shang, M. Medarde, J. S. White, and E. Pomjakushina, Phys. Rev. Materials **3**, 024204 (2019).
[32] S. Bobev, P. H. Tobash, V. Fritsch, J. D. Thompson, M. F. Hundley, J. L. Sarrao, and Z. Fisk, J. Solid State Chem. **178**, 2091 (2005).
[33] S. Mangin, D. Ravelosona, J. A. Katine, M. J. Carey, B. D. Terris, and E. E. Fullerton, Nat. Mater. **5**, 210 (2006).
[34] V. Franco, J. Blázquez, and A. Conde, Appl. Phys. Lett. **89**, 222512 (2006).
[35] S. S. Samatham and V. Ganesan, Phys. Rev. B **95**, 115118 (2017).
[36] J. Fan, L. Pi, L. Zhang, W. Tong, L. Ling, B. Hong, Y. Shi, W. Zhang, D. Lu, and Y. Zhang, Appl. Phys. Lett. **98**, 072508 (2011).
[37] V. K. Pecharsky and K. A. Gschneidner Jr., J. Magn. Magn. Mater. **200**, 44 (1999).
[38] D. Griffiths, *Introduction to Electrodynamics*, 3rd ed. (Prentice Hall, Englewood Cliffs, NJ, 1999), pp. 559–562.
[39] V. Franco, A. Conde, J. Romero-Enrique, and J. Blázquez, J. Phys.: Condens. Matter **20**, 285207 (2008).
[40] V. Franco and A. Conde, Int. J. Refrig. **33**, 465 (2010).
[41] L. P. Kadanoff, Physics **2**, 263 (1996).
[42] A. Arrott and J. E. Noakes, Phys. Rev. Lett. **19**, 786 (1967).
[43] B. Widom, J. Chem. Phys. **43**, 3898 (1965).
[44] R. B. Griffiths, Phys. Rev. Lett. **23**, 17 (1969).
[45] H. E. Stanley, *Introduction to Phase Transitions and Critical Phenomena* (Oxford University Press, London, 1971).
[46] P. Puphal, S. Krebber, E. Suard, R. Cubitt, C. Wang, T. Shang, V. Ukleev, J. S. White, and E. Pomjakushina, Phys. Rev. B **101**, 214416 (2020).
[47] S. N. Kaul, J. Magn. Magn. Mater. **53**, 5 (1985).
[48] J. C. Le Guillou and J. Zinn-Justin, Phys. Rev. B **21**, 3976 (1980).
[49] K. Huang, *Statistical Mechanics*, 2nd ed. (Wiley, New York, 1987).
[50] N. Tateiwa, J. Pospíšil, Y. Haga, and E. Yamamoto, Phys. Rev. B **97**, 064423 (2018).
[51] P. Opletal, V. Sechovský, and J. Prokleška, Phys. Rev. B **102**, 224438 (2020).
[52] W. Kleemann, J. Dec, V. V. Shvartsman, Z. Kutnjak, and T. Braun, Phys. Rev. Lett. **97**, 065702 (2006).
[53] P. Puphal, V. Pomjakushin, N. Kanazawa, V. Ukleev, D. J. Gawryluk, J. Ma, M. Naamneh, N. C. Plumb, L. Keller, R. Cubitt, E. Pomjakushina, and J. S. White, Phys. Rev. Lett. **124**, 017202 (2020).
[54] Y. Wang, J. H. Yu, Y. Q. Wang, C. Y. Xi, L. S. Ling, S. L. Zhang, J. R. Wang, Y. M. Xiong, T. Han, H. Han, J. Yang, J. Gong, L. Luo, W. Tong, L. Zhang, Z. Qu, Y. Y. Han, W. K. Zhu, L. Pi, X. G. Wan *et al.*, Phys. Rev. B **97**, 115133 (2018).
[55] M. Neupane, M. M. Hosen, I. Belopolski, N. Wakeham, K. Dimitri, N. Dhakal, J.-X. Zhu, M. Z. Hasan, E. D. Bauer, and F. Ronning, J. Phys.: Condens. Matter **28**, 23LT02 (2016).